Molecular basis of calcium regulation in connexin-32 hemichannels

Juan M. Gómez-Hernández*, Marta de Miguel*, Belen Larrosa, Daniel González, and Luis C. Barrio†

Unit of Experimental Neurology, Research Department, ''Ramón y Cajal'' Hospital, Carretera de Colmenar Viejo km 9, 28034 Madrid, Spain

Edited by Michael V. L. Bennett, Albert Einstein College of Medicine, Bronx, NY, and approved October 13, 2003 (received for review January 20, 2003)

In addition to forming gap-junction channels, a subset of connexins (Cxs) also form functional hemichannels. Most hemichannels are activated by depolarization, and opening depends critically on the external Ca^{2+} concentration. Here we describe the mechanisms of action and the structural determinants underlying the Ca^{2+} regulation of Cx32 hemichannels. At millimolar calcium concentrations, hemichannel voltage gating to the full open state of ≈90 pS is inhibited, and ion conduction at negative voltages of the partially open hemichannels (≈18 pS) is blocked. Thus, divalent cation blockage should be considered as a physiological mechanism to protect the cell from the potentially adverse effects of leaky hemichannels. A ring of 12 Asp residues within the external vestibule of the pore is responsible for the binding of Ca^{2+} that accounts for both pore occlusion and blockage of gating. The residue Asp-169 of one subunit and the Asp-178 of an adjacent subunit must be arranged precisely to allow interactions with Ca^{2+} to occur. Interestingly, a naturally occurring mutation (D178Y) that causes an inherited peripheral neuropathy induces a complete Ca^{2+} deregulation of Cx32 hemichannel activity, suggesting that this dysfunction may be involved in the pathogenesis of the neuropathy.

Vertebrate gap-junction channels are made up of connexins (Cxs), a gene family encoding at least 20 different isoforms (1). Each gap-junction channel is built up by the docking of two hemichannels, one from each of the neighboring cells. In addition to contributing to gap-junction channels, a subset of Cxs make open hemichannels in the plasma membrane that are capable of fulfilling a role other than that of gap-junction-mediated cell-to-cell communication. Cxs oligomerize into hexameric structures, i.e., hemichannels, before reaching the cell surface (2), and thus the presence of undocked hemichannels in the plasma membrane constitutes a normal phase in the life cycle of gap-junction proteins. Although it was thought that hemichannels remained closed in the plasma membrane until a newly formed channel acquires an open configuration, analysis of rat Cx46 in *Xenopus* oocytes revealed that the hemichannels can be voltage-gated by depolarization in the nonjunctional plasma membrane under physiological conditions (3). It is now known that this capacity to form functional hemichannels is widely extended among members of the Cx family, and that functional hemichannels are present in many native cells (4–7).

Hemichannels permit the rapid exchange of ions and of small molecules between the cytoplasm and the extracellular space (8–12). As such, they have been implicated in the regulation of various physiological processes (11, 13–15), as well as in the pathogenesis of certain disorders (16–19). The activation of hemichannels depends critically on the external Ca^{2+} concentration ($[Ca^{2+}]_o$). External Ca^{2+} ions are known to affect the voltage sensitivity of gating (20, 21) and can induce reversible conformational changes of hemichannel structure, compatible with a mechanism of gating (22). However, the molecular basis for this regulation remains unknown. We show here that the direct interaction of divalent cations with a site in the external vestibule of the pore mediates most Ca^{2+} effects on the Cx32 hemichannels. This binding site is responsible for preventing voltage-gated opening of hemichannels to the higher conductance sublevel (90 pS) and also for blocking inward currents through the lower conductance open state (18 pS). Thus, divalent cation blockage is a prominent feature in the physiology of Cx32 hemichannels. We also report that in a Cx32 mutant associated with a hereditary peripheral neuropathy, this binding site is destroyed, causing the complete Ca^{2+} deregulation of these hemichannels.

Methods

Construction of Mutants. Missense mutations were introduced into wild-type human Cx32 cDNA in a pBSXG vector (18) by site-directed point mutagenesis by using PCR primers that annealed back-to-back and amplified the whole plasmid. The primers used were: E47Q, sense 5′-AAA TCT TCC TTC ATC TGC AAC ACA-3′ and antisense 5′-CT*G* ATC ACC CCA CAC ACT CTC-3′ creating a new *Bcl*I site; D66N, sense 5′-TAT *A*AC CAA TTC TTC CCC ATC TC-3′ and antisense 5′-GCA *G*AC GCT GTT GCA GCC AGG-3′, creating a new *Alw*NI site; D169N, sense 5′-*A*AC GTC TAC CCC TGC CCC AAC-3′ and antisense 5′-GCA CTT GAC CAG CCG CAC CAT-3′, suppressing a *Aat*II site; D178N, sense 5′-*A*AC TGC TTC GTG TCC CGC C-3′ and antisense 5′-CAC TGT GTT GGG GCA GGG GT-3′, destroying a *Bst*XI site; and D178Y, sense 5′-*T*AC TGC TTC GTG TCC CGC C-3′ and antisense 5′-CAC TGT GTT GGG GCA GGG GT-3′, removing a *Bst*XI site. Mutants were screened by restriction enzyme analysis, and the mutations were confirmed by sequencing.

Electrophysiology. Oocytes from *Xenopus laevis* were prepared as described (18). Oocytes were coinjected with antisense oligonucleotides against *Xenopus* Cx38 mRNA, anti-Cx38, to block endogenous expression (10 ng per oocyte; ref. 23) and with the *in vitro* transcribed cRNA of wild-type or mutated Cx32 (0.1–0.5 $\mu g/\mu l$). Whole membrane currents were measured in isolated oocytes by the conventional two-electrode voltage–clamp method. Although specific blockers are not available, the currents induced in wild-type and mutant Cx32 injected oocytes could be mainly attributed to the activation of Cx32 hemichannels (see ref. 18 and Fig. 5, which is published as supporting information on the PNAS web site). The external ND96 solution for recording contained (in mM): 96 NaCl, 2 KCl, 1 $MgCl_2$, 1.8 $CaCl_2$, and 5 Hepes (pH 7.4). The low Ca^{2+} solution was 100 mM NaCl/2 mM KCl/0.5 mM $CaCl_2$/5 mM Hepes, pH 7.4. Smaller concentrations of divalent cations were avoided because the nonselective leak conductance of oocytes increases. Hemichannel conductance (g_{hj}) was normalized to the maximal value obtained at low Ca^{2+} in the same oocyte ($g_{hj0.5}$), and the mean average values were fitted to the following equation:

This paper was submitted directly (Track II) to the PNAS office.

Abbreviations: Cx, connexin; $[Ca^{2+}]_o$, external Ca^{2+} concentration; CMTX, X-linked Charcot–Marie–Tooth disease; SIS, standard internal solution.

*J.M.G.-H. and M.d.M. contributed equally to this work.

†To whom correspondence should be addressed. E-mail: luis.c.barrio@hrc.es.

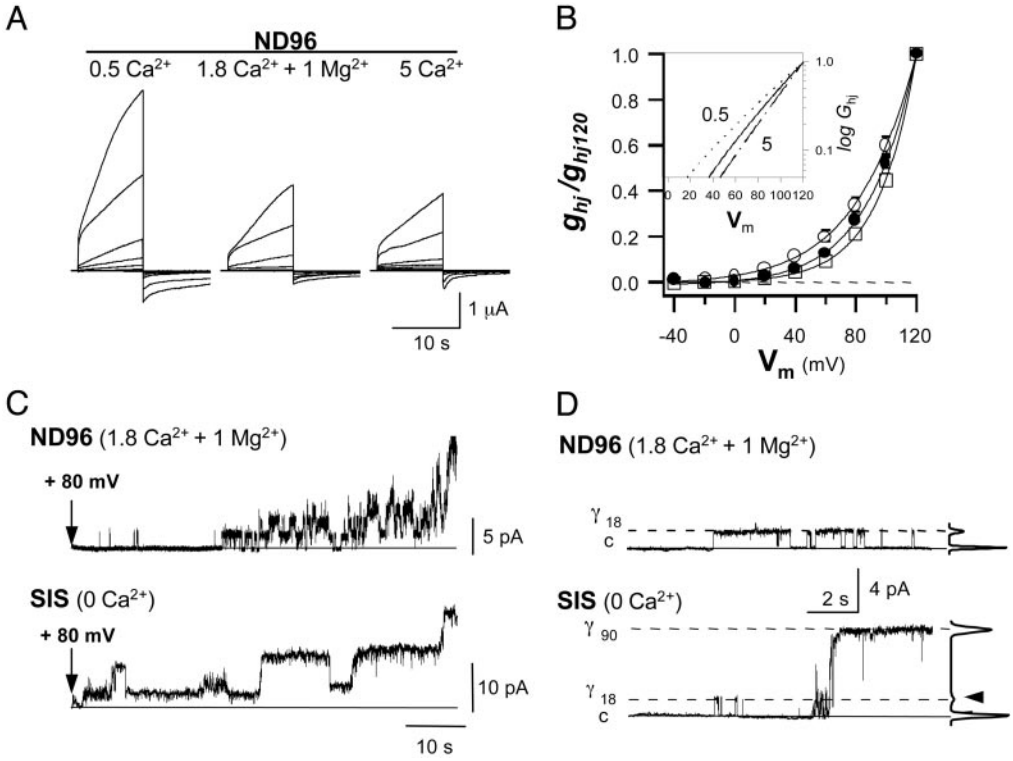

Fig. 1. External Ca^{2+} blocks full voltage-gated opening of human Cx32 hemichannels. (*A*) Slowly activating outward currents evoked by depolarizing pulses in isolated Cx32 *Xenopus* oocytes exposed to normal (ND96, 1.8 mM Ca^{2+} and 1 mM Mg^{2+}), low (0.5 mM), and high $[Ca^{2+}]_o$ (5 mM) solutions. Pulses of 10 s were applied from −40 to +120 mV in 20-mV increments. (*B*) Changes in the activation curve (mean ± SD; $n = 6$) and limiting voltage sensitivity (*Inset*) with $[Ca^{2+}]_o$ (ND96, ● and continuous line; 0.5 mM Ca^{2+}, ○ and dotted line; and 5 mM Ca^{2+}, □ and broken line). Macroscopic hemichannel conductance (g_{hj}) was calculated for the currents at the end of the 10-s pulses for a reversal potential of −5 mV and normalized relative to the value at +120 mV (g_{hj120}). (*C*) Macropatch records in cell-attached configuration of Cx32 hemichannels. With a normal external solution (ND96) in the pipette, after a delay, hemichannel activation at +80 mV resulted in frequent progressive transitions between the closed and open states of an increasing number of open hemichannels. When hemichannels were exposed to internal solution (SIS) without additional Ca^{2+}, activation involved much longer open times and much higher unitary currents. (*D*) Records containing a single open hemichannel at +80 mV and histogram amplitude. The main open conductance level of hemichannels in a ND96 solution was of 18.0 ± 0.4 pS (γ_{18}), whereas in a divalent cation-free solution (SIS), the dominant open state was of 87.2 ± 1.7 pS (γ_{90}), and less frequent transitions to γ_{18} were also detected (arrow).

$$g_{hj} = g_{hj0.5}/(1+\{[Ca^{2+}]_o/EC_{50}\}^{nhill}),$$

where EC_{50} is the half-maximal inhibition, and *nhill* is the Hill coefficient. Fits were made by treating these constants as free parameters. Patch–clamp experiments were performed according to standard techniques (18). Standard internal solution (SIS) contained (in mM): 100 KCl, 10 Hepes, and 10 EGTA, pH 7.2. Borosilicate glass pipettes (Dagan Instruments, Minneapolis) with a resistance of 1.5–4 MΩ were filled with ND96 or SIS solution, and the bath solution was SIS. Under these conditions, the membrane potential of the oocytes was near zero, as confirmed by the lack of appreciable differences in unitary conductance and the reversal potential of hemichannels in the cell-attached and excised configurations. Unitary records were filtered at 200 Hz and 1 kHz and sampled at 1 and 4 kHz, respectively.

Results

Two Specific Mechanisms Through Which External Ca^{2+} Can Regulate Cx32 Hemichannels. At physiological concentrations of external divalent cations, human Cx32 hemichannels expressed in *Xenopus* oocytes are capable of undergoing voltage-gated opening (18). Variations in $[Ca^{2+}]_o$ produced a complex regulation of hemichannel currents at the macroscopic and unitary levels. In a normal external solution (ND96, containing 1.8 mM Ca^{2+} and 1 mM Mg^{2+}), depolarizing pulses applied to Cx32 oocytes induced characteristic slowly activating outward currents. Currents increased with the degree of depolarization and did not reach saturation within the time and voltage range explored (Fig. 1*A*). Returning to the holding potential at −40 mV, the currents became inward and closed over a slow time course. In these experiments, the whole membrane currents were mainly attributable to Cx32 hemichannel activation (see Fig. 5). However, when the $[Ca^{2+}]_o$ was increased to 5 mM, the amplitude of the macroscopic hemichannel currents decreased (Fig. 1*A*), in agreement with the small shift of the activation curve toward more positive voltages and a ≈15-mV increment in the threshold (Fig. 1*B*). These changes in voltage sensitivity could be due to divalent cation screening of the surface charge (24). However, lowering the $[Ca^{2+}]_o$ to 0.5 mM increased the amplitude of depolarization induced currents 2- to 3-fold (Fig. 1*A*). This increase was much greater than might be expected for smooth changes in the gating sensitivity, the negative shift of the activation curve along the voltage axis, and the threshold reduction of ≈17 mV (Fig. 1*B*).

In cell-attached configuration, the single-channel records of membrane patches containing multiple and unique hemichannels displayed properties consistent with those observed at the macroscopic level. At normal divalent cation concentrations, activation occurred through a series of recurrent transitions mainly between the closed state and the main open state, and the number of open hemichannels tended to increase slowly and progressively during the pulse (Fig. 1*C*, ND96). The unitary conductance of the main open state was 18.0 ± 0.4 pS, γ_{18} (Fig.

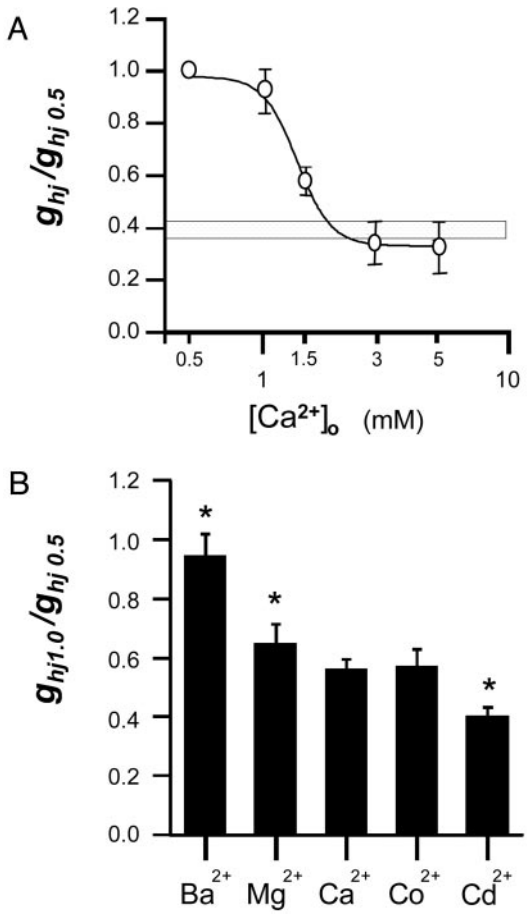

Fig. 2. Effects of extracellular Ca^{2+} and other divalent cations on hemichannel conductance. (*A*) Dose–response curve for $[Ca^{2+}]_o$ (mean ± SD; $n = 8$). Calcium chloride was added to the low-Ca^{2+} solution (0.5 mM) to achieve the final concentrations. The macroscopic hemichannel conductance (g_{hj}) was normalized to the value obtained at low Ca^{2+} in the same oocyte ($g_{hj0.5}$). Hemichannel conductance in normal external solution (ND96, 1.8 Ca^{2+} and 1 Mg^{2+}) is indicated (horizontal bar). Data were fitted to the Hill equation with an EC_{50} of 1.3 mM and a Hill coefficient of 6.3. (*B*) Blocking potency of different divalent cations (mean ± SD; $n = 6$). The degree of inhibition ($g_{hj1.0}/g_{hj0.5}$) was estimated when 1 mM of divalent ions was added to the low 0.5 mM Ca^{2+} solution ($n = 6$). Asterisks indicate significant differences relative to 1.5 mM Ca^{2+} (*t* test, $P < 0.05$).

1*D*, ND96). In low $[Ca^{2+}]_o$ conditions (ND96 with only 0.5 mM Ca^{2+} or SIS without additional Ca^{2+}), hemichannel activation in the macropatch was characterized by less frequent transitions between the different conductance states, much longer open times, and the opening of hemichannels to a main unitary conductance of 87.2 ± 1.7 pS, γ_{90} (Fig. 1 *C* and *D*, SIS; and Fig. 6, which is published as supporting information on the PNAS web site, 0.5 mM Ca^{2+}). Although opening to the γ_{90} state was never observed in a normal external solution, the γ_{18} conductance sublevel (the main open state in the normal solution) was still detected in the absence of Ca^{2+}. Thus, the data suggest that external Ca^{2+} blocks voltage gating of Cx32 hemichannels to the fully open state, γ_{90}.

At the macroscopic level, the dose–response curve varied between a maximum at 0.5 mM and a minimum at 3–5 mM $[Ca^{2+}]_o$ (representing 35% of the maximal conductance estimated at the end of 10-s depolarization), and an EC_{50} of 1.3 mM was observed (Fig. 2*A*). Note that the value of hemichannel conductance in normal external solution (ND96 with 1.8 mM Ca^{2+} and 1 mM Mg^{2+}) fell close to the minimum of the curve. The kinetics of the Ca^{2+}-induced changes were slow, with time constants in the range of 1–5 min (data not shown). Substitution of Ca^{2+} in the external solution with other divalent cations also inhibited Cx32 hemichannel activation. The potential of different divalent cations to induce such a block follows the sequence: $Cd^{2+} > Co^{2+} \approx Ca^{2+} > Mg^{2+} > Ba^{2+}$ (Fig. 2*B*).

Hemichannel currents activated by positive voltages were outward. Currents became inward, crossing the reversal potential near −5 mV, then decreased in a voltage-dependent manner at negative potentials (Fig. 3*A*). Moreover, the degree of curvature varied with the $[Ca^{2+}]_o$. Indeed, although the I–V relationship of macroscopic currents was almost a straight line when the $[Ca^{2+}]_o$ was lowered to 0.5 mM, rectification increased with 5 mM $[Ca^{2+}]_o$. At the single-channel level, the γ_{18} unitary currents showed characteristic high-frequency interruptions at negative voltages with a normal ND96 solution (Fig. 3*B Inset*). Deactivation of the tail currents at −40 mV involved burst activity between the closed and the γ_{18} open state, with brief opening times of very fast fluctuating unitary currents that alternated with progressive longer silent periods (Fig. 3*C*, ND96). With an internal SIS solution free of Ca^{2+} and Mg^{2+} (Fig. 3*C*) or in low external ND96 solution with only 0.5 mM Ca^{2+} (Fig. 6), deactivation first showed opening to the higher conductance state (γ_{90}) without flickering interruptions, followed by partial closure to the γ_{18} open state where the hemichannel stayed open without flickering for many seconds before closing fully. These data at the macroscopic and single-channel level indicate that external Ca^{2+} partially blocks inward current flow through Cx32 hemichannels but only when the hemichannel remained open at the smaller conductance sublevel (γ_{18}).

Molecular Determinants for Ca^{2+} Binding. Topologically, Cx32 contains four α-helix transmembrane domains (M1–M4), the N and C termini, an intermediate cytoplasmic loop, and two extracellular loops (E1 and E2). However, it remains unclear which of the specific domains in the Cx molecule contribute to the external vestibule of the pore. To identify the Cx32 residues that interact with Ca^{2+}, we introduced substitutions in the E1 loop (E47Q and D66N) and in the E2 domain (D169N and D178N), replacing carboxylate-containing residues with polar uncharged amino acids. Although none of these substitutions interfered with the ability to make hemichannels, the D169N and the D178N hemichannels responded to voltage pulses by producing less variable amplitudes of macroscopic currents than those observed in wild-type hemichannels exposed to changes in $[Ca^{2+}]_o$ (i.e., the changes at 0.5 mM Ca^{2+} were not so large; Fig. 4*A*). This reduction in Ca^{2+} sensitivity was similar for both mutants (Fig. 4*B*).

In patches exposed to normal ND96 solution, replacement of the negatively charged D169 or D178 with a neutral Asn residue dramatically altered the single-channel properties in two ways. First, on depolarization, the D169N or D178N hemichannel opened to both γ_{18} and γ_{90} conductance sublevels; and second, the flickering interruptions of the γ_{18} unitary currents disappeared at negative voltages (Fig. 4*C*). Thus, in normal $[Ca^{2+}]_o$, the D169N and D178N hemichannels behaved as wild-type hemichannels in the absence of divalent cations. Interestingly, the replacement of Asp-178 by Tyr is a naturally occurring mutation associated with the X-linked form of Charcot–Marie–Tooth disease (CMTX) (25). On analysis, the CMTX hemichannels were similarly insensitive to $[Ca^{2+}]_o$ (Fig. 4*B*), and at normal $[Ca^{2+}]_o$, full opening was not prevented nor was ion conduction through the partially open hemichannels blocked (Fig. 4*C*). Taken together, the results strongly indicate that both the Asp residues, D169 and D178, are necessary for Ca^{2+} binding, and that the same binding site mediates both pore occlusion and voltage-gated blockage.

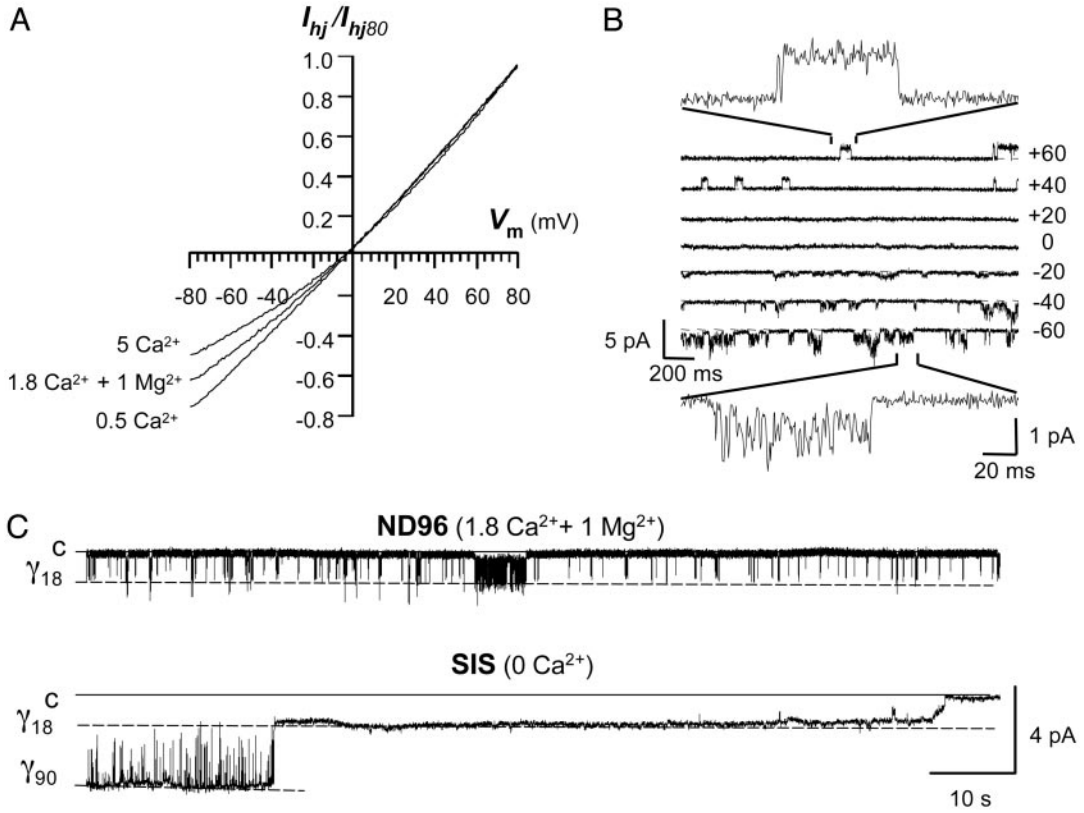

Fig. 3. External Ca^{2+} blocks ion conduction through the partially open Cx32 hemichannels in a voltage- and concentration-dependent manner. (*A*) Macroscopic I–V relationship in normal (ND96, 1.8 Ca^{2+} and 1 Mg^{2+}), low (0.5 mM), and high (5 mM) Ca^{2+} solutions. The voltage was held at +80 mV during 30 s to activate the hemichannels; it was then reduced to −80 and ramped upward from −80 to +80 mV in 250-ms steps. Each curve represents the average of four successive ramps after leak current subtraction. (*B*) Raster plot of unitary tail currents of hemichannels previously activated (+80 mV, 5 s) and recorded in cell-attached mode with a normal ND96 solution in the patch pipette. Note the flickering interruptions of unitary events at negative voltages (*Insets*). (*C*) Records of unitary tail currents at −40 mV of hemichannels activated as in *B*. In normal external solution (ND96, 1.8 Ca^{2+} and 1 Mg^{2+}), only unitary events of 18 pS were observed. Deactivation progressed as frequent and recurrent transitions between the fully closed (c) and open states (γ_{18}), with brief opening times of very fast fluctuating unitary currents alternated with longer silent periods. In the internal solution (SIS, 0 Ca^{2+}), the records initially showed a very stable γ_{90} state that closed to a long-lasting open γ_{18} state before finally closing completely.

Because each Cx32 hemichannel is formed by six Cx subunits, the Ca^{2+}-binding site may be composed of D169 and D178 residues belonging to the same extracellular E2 loop or to adjacent subunits. To discern between these two possibilities, equal amounts of RNA for the two single D169N and D178N mutants were coinjected into oocytes. Interestingly, the formation of heteromeric D169N and D178N hemichannels was able to rescue most of the Ca^{2+}-dependent properties. The Ca^{2+} sensitivity of the resulting average hemichannel population conductances fell between the curves of the wild type and that of each mutant alone (Fig. 4*B*, triangles), indicating that the interaction of D169 and D178 from adjacent Cx subunits is required for Ca^{2+} binding, and indeed, unitary records supporting this conclusion could be observed. At normal $[Ca^{2+}]_o$, some hemichannels (13/51) opened only to the γ_{18} state on depolarization (+80 mV), and at negative voltages (−40 mV), inward currents showed flickering interruptions (Fig. 4*D*).

Discussion

This study identifies the molecular mechanisms and structural determinants by which Ca^{2+} regulates Cx hemichannels. We have identified a Ca^{2+}-binding site, with millimolar affinity, within the extracellular vestibule of the pore of Cx32 hemichannels. Through this binding site, Ca^{2+} can block both voltage-gated opening to the higher conductance open state (γ_{90}) and ion conduction through the partially open hemichannels (γ_{18}).

The binding of Ca^{2+} appears, as in other ion channel families, to be a generic property of carboxylate clusters provided by adjacent Asp residues. The ring of 12 Asp identified in hexameric Cx32 hemichannels resembles the set of four Glu residues that form the "EEEE locus" of the four homologous repeats of the α_1 subunit of L-type Ca^{2+} channels (26) or the tetrameric cGMP-gated channel subunits (27). In Cx32 hemichannels, each Cx subunit contributes two Asp residues to this domain, because the neutralization of either of the two Asp in the E2 loop, D169 or D178, was sufficient to abolish both types of Ca^{2+} blockage (Fig. 4*C*). Moreover, the dual block was partially recovered in heteromeric hemichannels containing the two mutant subunits (Fig. 4*D*). This recovery suggests that the D169 residue of the D178N subunit and the D178 from the adjacent D169N subunit must be arranged in a precise way to allow the interaction with Ca^{2+} to occur. Taken together, the data indicate that each wild-type Cx32 hemichannel may contain up to six Ca^{2+}-binding sites. Furthermore, the occupancy of three of these sites would be sufficient to partially occlude the lumen and block full voltage gating, because this is the maximal number of theoretical binding sites that could result from the combination of the two mutant subunits in heteromeric D169N and D178N hemichannels (see Fig. 7 and *Supporting Discussion 1*, which are published as supporting information on the PNAS web site).

Single-channel analysis of Cx32 hemichannels suggests that there are two different gates that mediate the transitions be-

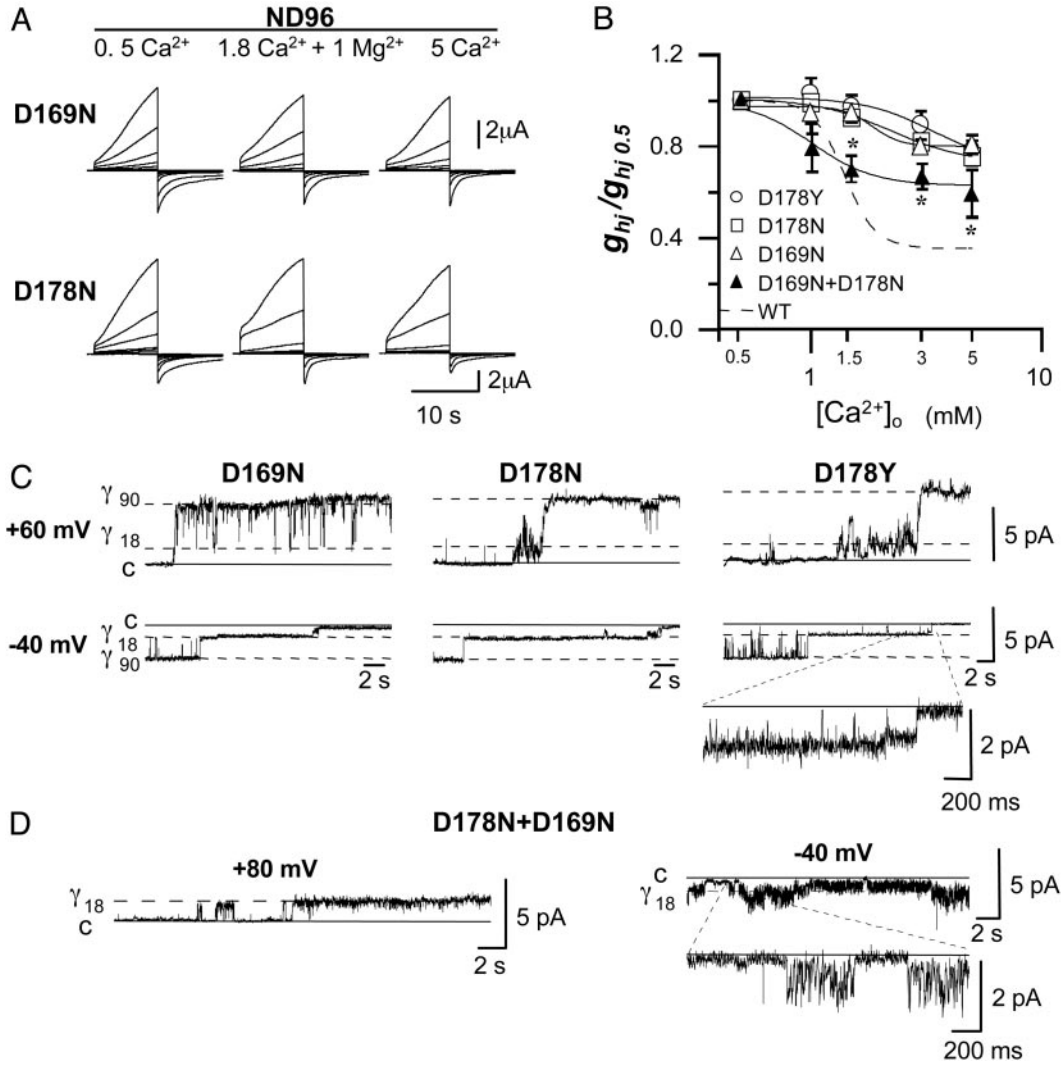

Fig. 4. Two Asp residues (D169 and D178), one from each of the adjacent Cx32 subunits, mediate the Ca^{2+}-induced blockage of voltage gating and pore conduction. (*A*) Slow-activating outward currents of the single neutralizing D169N and D178N mutant hemichannels elicited by the voltage-pulse protocol of Fig. 1*A* in normal (ND96), low (0.5 mM), and high (5 mM) Ca^{2+} solutions. Currents of both mutant hemichannels were no longer highly Ca^{2+}-dependent. (*B*) Dose–response curves for $[Ca^{2+}]_o$ (mean ± SD, $n = 6$). Data collection and fitting are as in Fig. 2*A*. Curves of homomeric mutant hemichannels (D169N, D178N, and D178Y) showed a large reduction in Ca^{2+} sensitivity vs. wild-type hemichannels (WT, broken line). The formation of heteromeric hemichannels by coexpressing the two mutant D169N and D178N subunits reintroduced moderate Ca^{2+} sensitivity; asterisks indicate significant differences relative to each mutant alone (*t* test, $P < 0.05$). (*C*) Single-channel recordings of homomeric mutant hemichannels (D169N, D178N, and D178Y) in a normal ND96 solution. All mutated hemichannels were capable of voltage gating to the fully open state (γ_{90}) at +60 mV, whereas at −40 mV, the inward currents of the partially open state (γ_{18}) did not show more flickery interruptions (*Inset*). Mutants behaved as wild-type hemichannels in the absence of external Ca^{2+}. (*D*) Selected unitary recordings of the oocytes coinjected with D169N and D178N mutants in a normal ND96 solution. A single hemichannel activated by a +80 pulse with exclusive opening to the lower γ_{18} conductance sublevel (*Left*) and showing the flickering γ_{18} currents during deactivation at −40 mV (*Right*).

tween the closed state and the low (γ_{18}) and high (γ_{90}) conductance sublevels. These two gates operate with the same polarity of voltage; both open on depolarization and close when the membrane potential repolarizes. However, they can be discriminated by the differential effects of Ca^{2+}. Divalent cations block the inward flow of current through partially open γ_{18} Cx32 hemichannels but not when they remain in the fully open state, γ_{90} (Figs. 3 and 4). It is conceivable that if the six putative binding sites were located near the narrowest constriction of the pore in the external vestibule, considered to be ≈5–7 Å in diameter (28, 29), then the binding of several Ca^{2+} ions of 2.1-Å diameter could cause the physical occlusion of the pore lumen, thereby compromising the inward flow of ions at negative voltages. This occlusion may disappear in the fully open state as a result of the gating motion. In this situation, the diameter pore may increase, and the two negative charges may be separated to the extent that they no longer form a binding site or they are no longer exposed. On the other hand, Ca^{2+} ions block gating only to the higher conductance state, γ_{90}, but not to the γ_{18} state (Figs. 1 and 2 *C* and *D*). Thus, this gate may correspond to that of gap-junctional channels under the control of transjunctional voltage because, at low Ca^{2+} concentrations, both close in a similar manner at the relatively negative voltage polarities between the same intervening states (Fig. 3*C* SIS and ref. 30; see *Supporting Discussion 2*, which is published as supporting information on the PNAS web site).

Our data indicate that the Ca^{2+}-dependent block of γ_{90} gating requires the presence of D169 and D178 from the E2 loops of adjacent subunits (Fig. 4 *C* and *D*). It has been postulated that the E2 loop forms a β-sheet stabilized by intramolecular disul-

phide bonds with the antiparallel β-sheet of the E1 loop (31). According to this model, the D169 and D178 residues that flank the $C64_{(E1)}$-$C168_{(E2)}$ and $C53_{(E1)}$-$C179_{(E2)}$ bridges could form multiple intermolecular Ca^{2+} bonds. Thus, they should stabilize the conformation between adjacent subunits, thereby blocking the motion of gating. In Cx43 channels, the 24 transmembrane α-helices of each hemichannel are packed in a left-handed bundle, with one notable exception: a single right-handed packing interaction for one of the two possible helix pairs that line the aqueous pore (28). This accounts for the narrowing of the pore at the extracellular gap. The tilting of this α-helix causes the other α-helix to be exposed to the pore in such a way that both α-helices contribute to the lining of the pore wall, thereby widening the pore diameter. By blocking this criss-cross arrangement, we speculate that Ca^{2+} binding could prevent the γ_{90} opening of Cx32 hemichannels. In support of this, Unwin and Ennis (32) described two Ca^{2+}-sensitive configurations of rat liver gap junction channels, which primarily contain Cx32, wherein the cytoplasmic domains of the subunits rotate, pivoting about a point close to the extracellular gap, thereby closing the hemichannel.

One conclusion arising from our study is that the binding site identified can account for the majority of the Ca^{2+}-dependent effects observed in Cx32 hemichannels. Only a small Ca^{2+}-sensitive component remained after the removal of this binding site by mutagenesis (Fig. 4*B*), which could be attributed to the unspecific effect of divalent cations in the voltage sensitivity of gating. The sequence alignment of the E2 Cx domains (see Table 1, which is published as supporting information on the PNAS web site) shows that the two-Asp motif is present in some, but not all, Cxs. Thus, more than one molecular mechanism for Ca^{2+} regulation of hemichannels might exist. Of the functional hemichannels so far described, mammalian Cx30, Cx46, Cx43, and *Xenopus* Cx38 are candidates to share the molecular model of Cx32.

Much remains to be discovered regarding the role played by Cx32 hemichannels and Ca^{2+} regulation in native cells. Although Cx32 is widely expressed in many tissues and cell types (1), in nervous tissue, it is preferentially expressed in oligodendrocytes (33), some specific neuronal populations (34), and the Schwann cells of peripheral nerves (35). Consistent with the millimolar affinity of the divalent cation-binding site identified, Cx32 hemichannels normally remain blocked under physiological conditions. However, below 0.5 mM $[Ca^{2+}]_o$, the undocked Cx32 hemichannels are no longer restrained by Ca^{2+} and will open to a $\approx$5-fold higher unitary conductance. Such abnormal decreases in $[Ca^{2+}]_o$ are associated with brain anoxia and spreading depression (36). Mutations in the Cx32 gene are the most frequent cause of the CMTX, an inherited motor and sensory peripheral neuropathy. More than 260 different mutations distributed throughout all of the topological domains of Cx32 have been detected in CMTX. Furthermore, the functional characterization of CMTX mutants has revealed the wide diversity of pathological mechanisms that cause this neuropathy. In this context, we show here that the D178Y mutant that destroyed the divalent cation-binding site caused a complete loss of the blocking actions exerted by Ca^{2+} on hemichannel activity (Fig. 4 *B* and *C*). This type of dysfunction may be relevant to the development of neuropathy because the uncontrolled opening of hemichannels would lead to a massive flux of ions and small molecules across the plasma membrane, producing adverse effects on Schwann cell viability. This hypothesis remains to be tested in future experiments.

We thank Gina Sosinsky and Juan Lerma for helpful discussions and Rosa Barquero for technical assistance. This work was supported by the European Commission (Grant QLG1-1999/00516 to L.C.B.), the Ministerio de Ciencia y Tecnología (Grant SAF2001-0048 to L.C.B.), and the Comunidad de Madrid (Grant 08.5/0069/2001 to L.C.B.). J.M.G.-H. is a "Ramón y Cajal" Program researcher.

1. Willecke, K., Eiberger, J., Degen, J., Eckardt, D., Romualdi, A., Güldenagel, M., Deutsch U. & Söhl, G. (2002) *Biol. Chem.* **383,** 725–737.
2. Musil, L. S. & Goodenough, D. A. (1993) *Cell* **74,** 1065–1077.
3. Paul, D. L., Ebihara, L., Takemoto, L. J., Swenson, K. I. & Goodenough, D. A. (1991) *J. Cell Biol.* **115,** 1077–1089.
4. Harris, A. L. (2001) *Q. Rev. Biophys.* **34,** 325–472.
5. Ebihara, L. (2003) *News Physiol. Sci.* **18,** 100–103.
6. Goodenough, D. A. & Paul, D. L. (2003) *Nat. Rev. Mol. Cell Biol.* **4,** 285–294.
7. Janssen-Bienhold, U., Schultz, K., Gellhaus, A., Schmidt, P., Ammermuller, J. & Weiler, R. (2001) *Visual Neurosci.* **18,** 169–178.
8. Li, H., Liu, T.-F., Lazrak, A., Peracchia, C., Goldberg, G. S., Lampe, G. P. & Johnson, R. G. (1996) *J. Cell. Biol.* **134,** 1019–1030.
9. Pfahnl, A., Zhou, X.-W., Werner, R. & Dahl, G. (1997) *Eur. J. Physiol.* **433,** 773–779.
10. Kondo, R. P., Wang, S.-Y., John, S. A., Weiss, J. N. & Golhaber, J. I. (2000) *J. Mol. Cell Cardiol.* **32,** 1859–1872.
11. Cotrina, M. L., Lin, J. H., Lopez-Garcia, J. C., Naus, C. C. & Nedergaard, M. (2000) *J. Neurosci.* **20,** 2835–2844.
12. Bruzzone, S., Guida, L., Zocchi, E. & DeFlora, A. (2001) *FASEB J.* **15,** 10–12.
13. Eckert, R., Donaldson, P., Goldie, K. & Kistler, J. (1998) *Invest. Ophthalmol. Visual Sci.* **39,** 1280–1285.
14. Kamermans, M., Fahrenfort, I., Schultz, K., Janssen-Bienhold, U., Sjoerdsma T. & Weiler, R. (2001) *Science* **519,** 1178–1180.
15. Plotkin, L., Stavros, L. I., Manolagas, S. C. & Bellido, T. (2002) *J. Biol. Chem.* **277,** 8648–8657.
16. John, S. A., Kondo, R., Wang, S. Y., Goldhaber, J. I. & Weiss, J. N. (1999) *J. Biol. Chem.* **274,** 236–240.
17. Contreras, J. E., Sanchez, H. A., Eugenin, E. A., Speidel, D., Theis, M., Willecke, K., Bukauskas, F. F., Bennett, M. V. L. & Saéz, J. C. (2002) *Proc. Natl. Acad. Sci. USA* **99,** 495–500.
18. Castro, C., Gómez-Hernández, J. M., Silander, K. & Barrio, L. C. (1999) *J. Neurosci.* **19,** 3752–3760.
19. Abrams, C. K., Bennett, M. V. L., Verselis, V. K. & Bargiello, T. A. (2002) *Proc. Natl. Acad. Sci. USA* **99,** 3980–3984.
20. Ebihara, L. & Steiner, E. (1993) *J. Gen. Physiol.* **102,** 59–74.
21. Pfahnl, A. & Dahl, G. (1999) *Eur. J. Physiol.* **437,** 345–353.
22. Müller, D. J., Hand, G. M., Engel, E. & Sosinsky, E. (2002) *EMBO J.* **21,** 3598–3607.
23. Barrio, L. C., Suchyna, T., Bargiello, T. A., Xu, L. X., Roginski, R. S., Bennett, M. V. L. & Nicholson, B. J. (1991) *Proc. Natl. Acad. Sci. USA* **8,** 8410–8414.
24. Hille, B. (1992) in *Ionic Channels of Excitable Membranes* (Sinauer, Sunderland, MA), pp. 445–471.
25. Bone, L. J., Deschênes, S. M., Balice-Gordon, R. J., Fischbeck, K. H. & Scherer, S. S. (1997) *Neurobiol. Dis.* **4,** 221–230.
26. Yang, J., Ellinor, P. T., Sather, W. A., Zhang, J. F. & Tsien, R. (1993) *Nature* **366,** 158–161.
27. Root, M. J. & MacKinnon, R. (1993) *Neuron* **11,** 459–466.
28. Unger, V. M., Kumar, N. L. Gilula, N. B. & Yeager, M. (1999) *Science* **283,** 1176–1180.
29. Oh, S., Ri, Y., Bennett, M. V. L., Trexler, E. B., Verselis, V. K. & Bargiello, T. A. (1997) *Neuron* **19,** 927–938.
30. Oh, S., Rubin, J. B., Bennett, M. V. L., Verselis, V. K. & Bargiello, T. A. (1999) *J. Gen. Physiol.* **114,** 339–364.
31. Foote, C. I., Zhou, L., Zhu, X. & Nicholson, B. J. (1998) *J. Cell Biol.* **140,** 1187–1197.
32. Unwin, P. N. T. & Ennis, P. D. (1984) *Nature* **307,** 609–613.
33. Rash, J. E., Yasumura, T., Dudeck, F. E. & Nagy, J. I. (2001) *J. Neurosci.* **21,** 1983–2001.
34. Venance, L., Rozov, A., Blatow, M., Burnasshev, N., Feldmeyer, D. & Moyer, H. (2000) *Proc. Natl. Acad. Sci. USA* **97,** 10260–10265.
35. Bergoffen, J., Scherer, S. S., Wang, S., Oronzi, M., Scott, L., Bone, J., Paul, D. L., Chen, K., Lensch, M. W., Chance, P. F., *et al.*. (1993) *Science* **262,** 2039–2042.
36. Somjen, G. G. (2001) *Physiol. Rev.* **81,** 1065–1096.